Metallophysics and Advanced Technologies
Металофіз. новітні технол.
Metallofiz. Noveishie Tekhnol.
2023, vol. 45, No. 4, pp. 431–441
https://doi.org/10.15407/mfint.45.04.0431
Reprints available directly from the publisher

PACS numbers: 61.43.Dq, 68.55.-a, 75.70.Ak, 76.50.+g, 81.15.Ef

Magnetic Properties of Fe_2CrGa Heusler Alloy Films

Yu. V. Kudryavtsev, V. O. Golub*, A. O. Perekos, T. G. Kabantsev*, M. P. Melnyk, and V. Yu. Tarenkov**

G. V. Kurdyumov Institute for Metal Physics, N.A.S. of Ukraine,
36 Academician Vernadsky Blvd.,
UA-03142 Kyiv, Ukraine
**Institute of Magnetism, N.A.S. and M.E.S. of Ukraine,*
36[b] Academician Vernadsky Blvd.,
UA-03142 Kyiv, Ukraine
***Donetsk Institute for Physics and Engineering Named after O. O. Galkin,*
N.A.S. of Ukraine,
46 Nauky Ave.,
UA-03028 Kyiv, Ukraine

Static and dynamical magnetic properties of the amorphous and crystalline $A2$-type ordered Heusler Fe_2CrGa-alloy films are investigated and compared with the properties of the bulk $A2$-type ordered Fe_2CrGa alloy. Unlike literature results for bulk Fe_2CrGa alloy, a complete structural disorder in amorphous state gives rise to a drastic decrease of alloy saturation magnetization. Annealing of amorphous films at $T_{ann} = 740$ K leads to their crystallization with the formation of the disordered $A2$-type structure and the magnetic properties of such crystalline films close to those of bulk alloy. Ferromagnetic resonance (FMR) investigations show that both amorphous and crystalline Fe_2CrGa-alloy films are microscopically inhomogeneous in both magnetic and structural aspects. Based on the FMR spectra analysis, it can be concluded that, in crystalline Fe_2CrGa-alloy films, there are regions with order close to the crystallographic $L2_1$ and Hg_2CuTi types. These results perfectly correlate with first-principal calculations of the magnetic properties of Fe_2CrGa alloy. As shown, the Slater–Pauling rule is not applicable for full Heusler alloys with inverse crystalline Hg_2CuTi-type structure.

Corresponding author: Yuriy Volodymyrovych Kudryavtsev
E-mail: kudr@imp.kiev.ua

Citation: Yu. V. Kudryavtsev, V. O. Golub, A. O. Perekos, T. G. Kabantsev, M. P. Melnyk, and V. Yu. Tarenkov, Magnetic Properties of Fe_2CrGa Heusler Alloy Films, *Metallofiz. Noveishie Tekhnol.*, **45**, No. 4: 431–441 (2023).
DOI: 10.15407/mfint.45.04.0431

Key words: thin magnetic films, amorphous state, atomic ordering, ferromagnetic resonance, Heusler alloys.

В роботі досліджено статичні та динамічні магнетні властивості аморфних і впорядкованих за типом $A2$ кристалічних плівок Гойслерового стопу Fe_2CrGa, яких порівняно з магнетними властивостями масивного стопу Fe_2CrGa зі структурою типу $A2$. На відміну від літературних даних для масивного стопу Fe_2CrGa атомовий безлад в аморфному стані стопу приводить до значного зменшення його намагнетованости наситу. Відпал аморфних плівок стопу Fe_2CrGa за температури $T_{від} = 740$ К спричинює кристалізацію їх з формуванням розупорядкованої структури типу $A2$ та відновлення намагнетованости наситу плівок до величин, близьких до намагнетованости масивного стопу. Дослідження феромагнетного резонансу (ФМР) показали, що як аморфні, так і кристалічні плівки стопу Fe_2CrGa у магнетному та кристалічному аспектах є неоднорідними. Виходячи з аналізи спектрів ФМР, зроблено висновок, що кристалічні плівки стопу Fe_2CrGa містять області, структура порядку в яких близька до $L2_1$- і Hg_2CuTi-типів. Ці висновки добре корелюють з результатами першопринципних розрахунків магнетних властивостей стопу Fe_2CrGa. Також показано, що правило Слетера–Полінґа не виконується для Гойслерових стопів із інверсною кристалічною структурою типу Hg_2CuTi.

Ключові слова: тонкі магнетні плівки, аморфний стан, атомове впорядкування, феромагнетний резонанс, Гойслерові стопи.

(Received 11 April, 2023; in final version, 13 April, 2023)

1. INTRODUCTION

One of the most remarkable features of X_2YZ (where X and Y are transition metals, Z is s–p metal) full Heusler alloys (HAs) with $L2_1$ type crystalline structure is ferromagnetic (FM) ordering of some alloys produced from «nonmagnetic» metals (like Cu_2MnAl or Cu_2MnSn) [1]. The FM behaviour of such HAs is due to FM coupling between «nonmagnetic» metals (Y like Mn or Cr) occupying specific positions in the HA lattice which makes them the third nearest neighbours (NN) separated by the distance of about third NN Mn–Mn ≈ 0.422–0.438 nm. Being in the second (second NN Mn–Mn ≈ 0.298–0.310 nm) or even the first (first NN Mn–Mn ≈ 0.211–0.219 nm) coordination sphere in the HA lattice these «nonmagnetic» metals are usually antiferromagnetically (AFM) coupled [2, 3]. Thus, it is clear that atomic order in HAs plays a crucial role in the formation of their resulting magnetic properties. If HA contains «ferromagnetic» metal (usually, Co, Fe, or Ni as X or/and Y) the situation becomes more complicated. In a disordered state, these «ferromagnetic» atoms can create their own clusters. A strong influence of the atomic order on the magnetic properties of HA has been shown experimentally and explained using the result of the

first-principal calculations of the electronic structure and magnetic properties of HAs [2, 4–14].

Probably Taylor and Tsuei were the first who obtained Cu_2MnZ (Z = In, Al, Sn) HA films in an amorphous state and showed their nonferromagnetic (or spin-glass) behaviour [4]. Krusin–Elbaum *et al.* explained the lack of FM ordering in an amorphous state of Cu_2MnZ (Z = In, Al, Sn) HA films in terms of competition between long-range indirect FM exchange with direct AFM overlap [2]. It was found that amorphous Ni_2MnGa HA films behave as Pauli paramagnet down to $T = 4.2$ K [6]. Annealing of such amorphous films restores their crystalline single-phase HA structure and FM properties typical for corresponding bulk alloys [4, 6]. At the same time, structural disorder induced by ball milling can significantly enhance the magnetization of bulk Fe_2CrGa alloy from ≈ 2.2 μ_B/f.u. up to 3.2–3.6 μ_B/f.u. [15]. Strong dependence of magnetic properties of Ni_2MnIn HA films on deposition temperature and post-annealing temperature (*i.e.* on the film structure) were also shown by Xie *et al.* [5]. The atomic disorder upon $L2_1$ to $A2$ order type transition in Co_2FeGe HA films leads to about 15% room temperature (RT) saturation magnetization reduction [7]. Kostenko and Lukoyanov theoretically considered the effect of atomic disorder on the electronic structure and magnetic properties of Fe_2VAl and Co_2CrAl HAs. It was shown that atomic disorder with a statistical distribution of defects or/and with the formation of some short-range order causes about 30% magnetic moment reduction in Co_2CrAl alloy and an appearance of the magnetic moment of about 1.9 μ_B/f.u. in nonmagnetic Fe_2VAl [13]. Ishida *et al.* considered the effect of various kinds of chemical disorder in Fe_2CrZ (Z = Si, Ge, Sn) HAs on their electronic structure and some physical properties. It was found that Fe–Z disorder causes 1.5–2.5 times increase in the total magnetic moment while Fe–Cr disorder leads to an insignificant increase or decrease in M_{tot} depending on Z [11].

The variation of the atomic order in the HA film samples usually can be achieved by changing the deposition temperature (RT or higher) and/or subsequent annealing. Vapour quenching deposition of the HA films onto substrates cooled by liquid nitrogen substrates allows fixing the chaos of the metallic atom distribution of a vapour phase in condensed films. In this study, the effect of atomic disorder on the magnetic properties of amorphous Fe_2CrGa alloy films has been investigated.

2. EXPERIMENTAL DETAILS

Bulk Fe_2CrGa alloy was prepared by melting together corresponding amounts of Fe, Cr, and Ga metals of 99.99% purity in an arc furnace with a water-cooled Cu hearth in 1.3 bar Ar atmosphere. The Ar gas in

the furnace before melting was additionally purified by multiple remelting of a $Ti_{50}Zr_{50}$ alloy getter. To promote volume homogeneity, the ingot was remelted five times. After ingot melting, the weight loss was found to be negligible. To obtain ordering of the alloy the ingot was annealed at $T = 1073$ K for 2 hours and slowly cooled down. The actual ingot composition was evaluated using energy dispersive x-ray spectroscopy and found to be $Fe_{51.8}Cr_{25.9}Ga_{22.2}$ (hereinafter Fe_2CrGa).

Fe_2CrGa alloy films with the thickness of about 100–180 nm were deposited from Fe_2CrGa alloy powder by flash evaporation in the vacuum better than $1 \cdot 10^{-4}$ Pa onto two glass substrates cooled down by liquid nitrogen. Vapour quenching deposition onto substrates cooled by liquid nitrogen was aimed to provide a complete structural disorder in the films. To obtain ordered state, one of the films from this couple was annealed at $T_{ann} = 740$ K in high vacuum.

Structural characterization of bulk and film samples was carried out at RT by Θ–2Θ x-ray diffraction (XRD) with CoK_α radiation ($\lambda = 0.179021$ nm). Static and dynamical magnetic properties of the bulk sample and films were investigated using vibrating sample Lake Shore 7404 magnetometer (VSM) and ferromagnetic resonance (FMR) spectroscopy on Bruker ELEXSYS-E500 spectrometer operating in x-range ($f = 9.864$ GHz). The standard resonance conditions for the external magnetic field applied perpendicular and parallel to the film plane are:

$$\frac{\omega}{\gamma} = H_{res}^{\perp} - 4\pi M_{eff}, \tag{1}$$

$$\frac{\omega}{\gamma} = \sqrt{H_{res}^{\parallel} \times (H_{res}^{\parallel} + 4\pi M_{eff})}. \tag{2}$$

Here, ω is frequency, $\gamma = (e/2mc)g$ is gyromagnetic ratio, g is Landé factor, M_{eff} is effective magnetization, $H_{res}^{\perp}$ and $H_{res}^{\parallel}$ are normal and in plane resonance magnetic fields, respectively [16]. Thus, M_{eff} for Fe_2CrGa alloy films can be extracted from the measured $H_{res}^{\perp}$ and $H_{res}^{\parallel}$ using the equations (1), (2).

3. RESULTS AND DISCUSSION

Figure 1 presents the experimental RT XRD patterns for the investigated bulk and film samples as well as simulated XRD stroke diagram for stoichiometric Fe_2CrGa alloy with $L2_1$ type of atomic order. Despite of the high-temperature annealing at $T_{ann} = 1073$ K, the disordered body-centred cubic (b.c.c.) $A2$ phase is formed in bulk Fe_2CrGa alloy sample—only fundamental (220), (400), and (422) reflections of the $L2_1$ phase (or (110), (200), and (211) ones for b.c.c. $A2$ phase) can be ob-

served (see Fig. 2). Its lattice parameter ($a_{L2_1} = 0.5823$ nm or $a_{A2} = 0.2911$ nm) is rather close to those reported in the literature: 0.5824 [17], 0.580–0.583 nm [15], and 0.5821 nm [18]. A vapour quenching deposition of the Fe_2CrGa alloy films onto liquid nitrogen cooled substrates results in the formation of totally amorphous state (see Fig. 1). Annealing of these amorphous Fe_2CrGa alloy films at $T_{ann} = 740$ K leads to film crystallization with an appearance of the reflections which are typical for the disordered b.c.c. $A2$ phase with the lattice parameter $a_{L2_1} = 0.58291$ nm (or $a_{A2} = 0.29145$ nm).

Thus, despite high temperature annealing we failed to obtain the $L2_1$ or even $B2$ phases in Fe_2CrGa alloy bulk and film samples. This experimental result correlates with unsuccessful attempts of Umetsu *et al.* to produce $L2_1$ or $B2$ type singe-phase samples of bulk Fe_2CrGa alloy and can be explained by theoretical results of Zhang *et al.* who revealed that the disordered $A2$ phase is more energetically preferable than the ordered $L2_1$ or $B2$ phases [18, 15].

Magnetic properties of the investigated bulk and film Fe_2CrGa alloy samples have been presented in Figs. 3–5 and summarized in Table 1. The $M(H)$ and $M(T)$ dependences for the bulk Fe_2CrGa alloy sample are typical for single-phase FM materials. The experimentally obtained value of the saturation magnetization for bulk Fe_2CrGa alloy sample is $M_{sat}(293\ K) = 1.9\ \mu_B$/f.u., which nicely correlates with the experi-

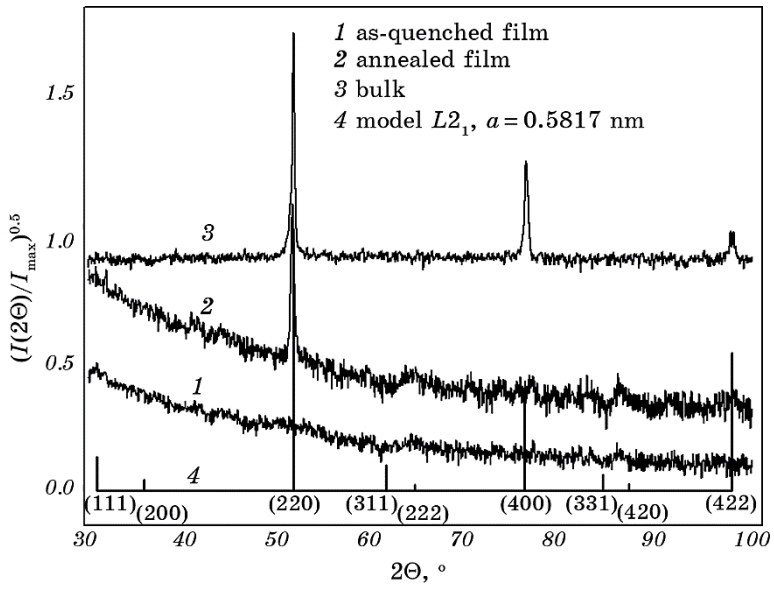

Fig. 1. RT experimental XRD patterns for bulk and film Fe_2CrGa alloy samples as well as simulated stroke-diagram for stoichiometric Fe_2CrGa alloy with $L2_1$ type atomic ordering.

mental results for bulk Fe_2CrGa alloy by Buschow ($M_{sat}(4.2\ K) = 2.6\ \mu_B$/f.u.), Zhang *et al.* [$2.2 \le M_{sat}(5\ K) \le 3.6\ \mu_B$/f.u.] and Umetsu *et al.* [$1.96 \le M_{sat}(4.2\ K) \le 2.67\ \mu_B$/f.u.] [17, 15, 18]. The Curie temperature of the bulk alloy $T_C = 416$ K also belongs to the interval determined by Umetsu *et al.* ($350 \le T_C \le 460$ K) for Fe_2CrGa alloy [18]. According to the results of first-principle calculations, the inverse Hg_2CuTi type of structure (space group 216) is more energetically preferable for stoichiometric Fe_2CrGa alloy than typical for most full HAs $L2_1$ one (space group 225) (see Fig. 2) [15, 19].

The inverse full HAs resemble the usual full HAs having also the chemical formula X_2YZ and crystallize in the so-called XA or Xα structure (the prototype structure is Hg_2CuTi) [20]. Usually, the inverse structure in full HAs is observed for alloys where the valence of the X transition atom is smaller than of the Y atom. The calculated magnetic moment of the stoichiometric Fe_2CrGa alloy with Hg_2CuTi structure type is more than two times larger than that of alloy with $L2_1$ structure type: $M(Hg_2CuTi) = 2.35$ or $2.20\ \mu_B$/f.u. *vs.* $M(L2_1) = 0.96$ or $1.00168\ \mu_B$/f.u. [15, 19]. For both these types, the ferrimagnetic coupling of magnetic moments is observed. However, for the case of $L2_1$ type of structure main magnetic moment is localized on Cr sites ($m_{Cr} = -1.43$ or $-1.60\ \mu_B$, $m_{Fe} = 0.25$ or $0.33\ \mu_B$) while for the case of Hg_2CuTi atomic order main contribution to the resulting magnetic moment of alloy comes from the Fe sites ($m_{FeI} = 1.74$ or $1.76\ \mu_B$, $m_{FeII} = 2.51$ or $2.52\ \mu_B$, $m_{Cr} = -1.69$ or $-1.89\ \mu_B$) [15, 19].

It is practically impossible to distinguish $L2_1$ and Hg_2CuTi structures from XRD measurements. The intensities of the (111) and (200)

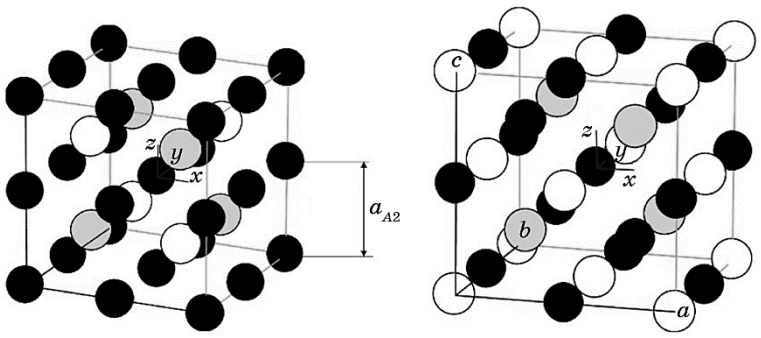

Fig. 2. Possible positions of Fe, Cr and Ga ions in stoichiometric Fe_2CrGa alloy with $L2_1$ (space group 225) or Hg_2CuTi (space group 216) types of atomic order. Fe, Cr and Ga ions are shown by black, grey, and white circles, correspondingly, a_{A2} is the lattice parameter for the case of random occupation of the lattice sites by Fe, Cr and Ga ions, *i.e.*, for $A2$ type of atomic order.

superstructure reflections for both perfectly ordered Hg_2CuTi and $L2_1$ phases do not exceed 4–6% of the amplitudes of the most intense (220) fundamental reflections. Furthermore, the intensities of the (111) and (200) superstructure reflections for both types of order differ insignificantly.

Based on the comparison of the results of the first-principle calculations and experimentally obtained magnetic data for the bulk Fe_2CrGa alloy it can be supposed a formation of the Hg_2CuTi type phase instead of the $L2_1$ one. It is well known that the Slater–Pauling rule allows predicting magnetic moment M_{s-p} for full Heusler alloys with typical for them $L2_1$ type of atomic structure [21–23]. According to this rule, M_{s-p} can be estimated as $M_{s-p} = (N_v - 24)\mu_B$, where N_v is the total number of valence electrons of full HA. For the case of Fe_2CrGa alloy, $N_v = 2(3d^6 + 4s^2)_{Fe} + (3d^5 + 4s^1)_{Cr} + (4s^2 + 3p^1)_{Ga} = 25$. Thus, according to Slater–Pauling rule, the resulting magnetic moment of Fe_2CrGa alloy should be equal to $M_{s-p} = (25 - 24)\mu_B = 1\mu_B$. It is easy to see that the experimentally obtained RT magnetization value of Fe_2CrGa bulk alloy is nearly two times larger than the predicted one. Skaftorous *et al.* have shown that the Slater–Pauling rule for inverse HAs should be material specific depending on the relative valence of X and Y atoms and may be presented as $M_{s-p} = (N_v - 18)\mu_B$, $M_{s-p} = (N_v - 24)\mu_B$ or $M_{s-p} = (N_v - 28)\mu_B$ [24]. So, M_{s-p} may be equal to +7, +1, or $-3\mu_B$/f.u., respectively. None of these values fit our case.

Magnetic measurements in the films have shown that structure disorder results in a drastic decrease of Fe_2CrGa saturation magnetization from $M_{cryst}(293\ K) = 160$ emu/cm^3 to $M_{amorph}(293\ K) = 19$ emu/cm^3 (see Fig. 3 and Table 1). Unlike bulk Fe_2CrGa alloy, there are two characteristic points on the temperature dependence of magnetization $M(T)$ of

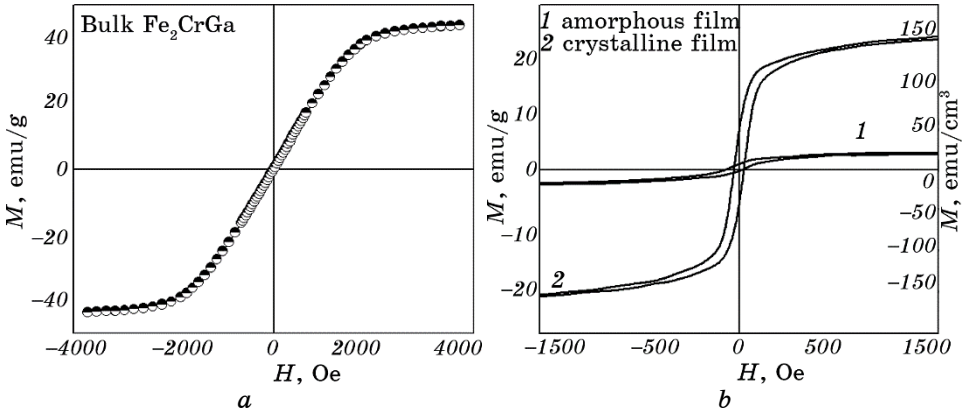

Fig. 3. RT magnetization hysteresis loops $M(H)$ for bulk (*a*) and film (*b*) (magnetic field is in the film plane) samples of Fe_2CrGa alloy.

crystalline Fe_2CrGa films at $T \approx 398$ and 470 K. Their appearance can be attributed to the coexistence of the several FM phases with different Curie temperatures in the film. Noisy $M(T)$ plot for amorphous Fe_2CrGa films (not shown) allowed only roughly evaluating their Curie temperature as $T_C \approx 400$ K.

The FMR absorption spectra for amorphous and crystalline Fe_2CrGa alloy films clearly show multipeak structure, which can be attributed to coexistence of the several magnetic phases with different values of the effective magnetization M_{eff} in the films (see Fig. 5). Multipeak analysis of the experimental FMR absorption spectra reveals the presence of at least 3-peaks with different positions of the absorption maxima. The investigation of the evolution of the FMR spectra with the deviation of the direction of external magnetic field from the film normal (polar angle) allowed to determine the contribution from these phases into the FMR spectra and to calculate the effective magnetizations M_{eff} for each phase using the equations (1) and (2). These results are presented in Table 1. Besides the paramagnetic phase, several FM phases ($M_{\text{eff}} = 1.26$ and $0.36\mu_B$/f.u.) were found in the amorphous film. While the VSM measurements gave the information about the mean saturation magnetization of the film, the FMR spectroscopy in the general case allows extracting parameters of individual phases. For

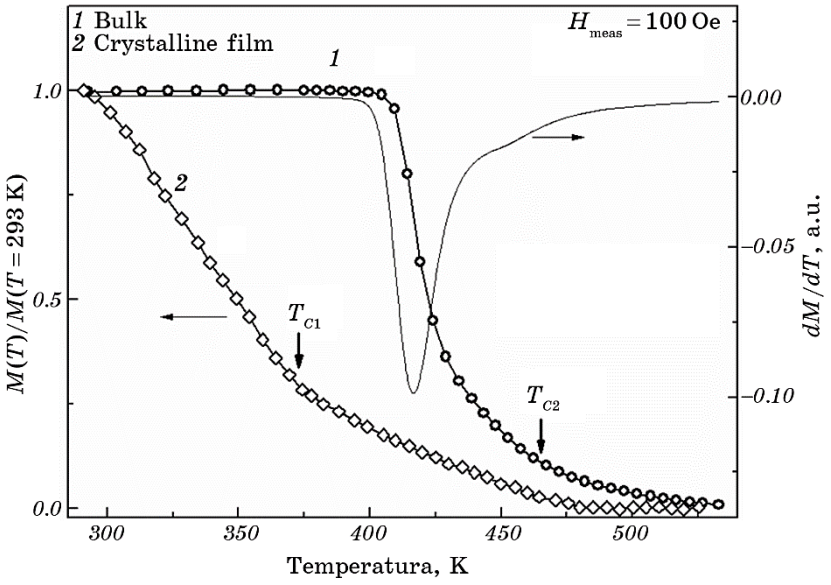

Fig. 4. Temperature dependences of magnetization normalized with respect magnetization at RT for bulk (*1*) and crystalline film (*2*) Fe_2CrGa alloy samples in the magnetic field $H_{\text{meas}} = 100$ Oe (symbols) (left scale). Line presents dM/dT dependence derived from $M(T)$ plot for bulk sample (right scale).

planar magnetic phases without magnetic anisotropy $M_{sat} = M_{eff}$. However, if we suppose that the amorphous film consist of the FM phases only its average saturation magnetization should be much higher than that extracted from VSM measurements.

The most probable explanation of this is that the magnetic clusters are embedded into paramagnetic matrix. It should be mentioned that in this case, the shape of such clusters can be far from plane and we cannot apply equations (1) and (2) for the determination of the saturation magnetization, but they can give us the information about low limit of the saturation magnetization of these phases. Crystallization of amorphous Fe_2CrGa films results in significant changes of the FMR absorption spectra as well as in nearly tenfold increase of M_{sat} (see Table 1). According to the FMR spectra analysis, the crystalline Fe_2CrGa films have regions with the local saturation magnetizations M_{eff} close to 1 and $2\mu_B$/f.u. Considering the results of first-principle calculations, it can be concluded that the crystallization of the films leads to the formation of different regions consisting of $L2_1$ or Hg_2CuTi phases. There are also regions with $M_{eff} = 0.75\mu_B$/f.u., which are needed to explain the net saturation magnetization $M_{sat} = 0.93\mu_B$/f.u. determined by VSM. The appearance of the nonmagnetic (paramagnetic) phase in amorphous Fe_2CrGa alloy films can be explained (by analogy with amorphous Cu_2MnSn films [2, 3]) by the interplay of FM and AFM couplings of the magnetic moments localized on Cr sites. As it was mentioned above, the resulting magnetic moment of $L2_1$ type Fe_2CrGa alloy is formed by FM coupled magnetic moments localized on Cr sites, which are the third nearest neighbours in $L2_1$ lattice. Being the first or second nearest neighbours in the amorphous film, the magnetic moments on Cr sites interact AFM. However, this rough qualitative ex-

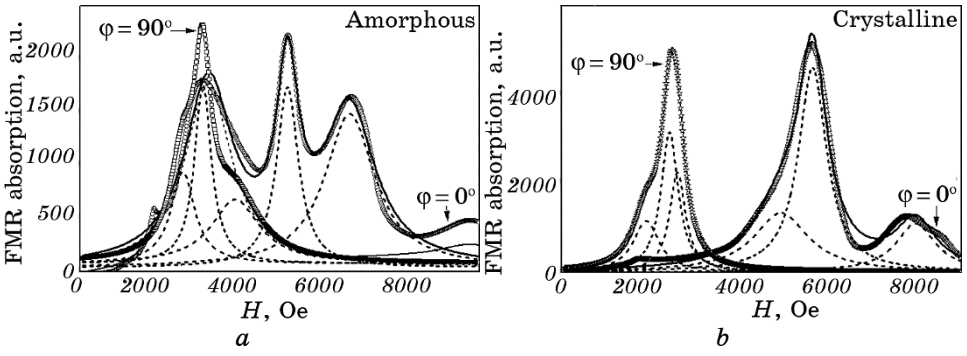

Fig. 5. RT FMR absorption spectra (symbols) for amorphous (*a*) and crystalline (*b*) Fe_2CrGa films recorded for the magnetic field directed perpendicular ($\varphi = 0°$) and parallel ($\varphi = 90°$) to the film plane. Solid and dashed lines show the results of multi-peak analyses of the experimental spectra.

TABLE 1. Experimentally determined magnetic properties of the investigated Fe_2CrGa samples.

Sample	T_{sub}, K	T_{ann}, K	Sample structure	M_{sat}(293 K), μ_B/f.u.	M_{eff}(293 K), μ_B/f.u.	T_C, K
Bulk		1073	Crystalline $A2$	1.9		416
Film	78	293	Amorphous	0.11	1.26 0.36 $\cong 0$	≈ 400
Film	78	740	Crystalline $A2$	0.93	2.07 1.05 0.75	≈ 480 ≈ 370 ?

planation does not consider the possibility of Fe cluster formation and their influence on the resulting magnetic properties of the alloy.

4. SUMMARY

1. Unlike bulk Fe_2CrGa alloy, a complete atomic disorder in amorphous films leads to dramatic decrease of the mean saturation magnetization. The comparison of FMR and magnetometry data allows proving the formation of large paramagnetic at RT regions in the amorphous films.
2. Amorphous and crystalline Fe_2CrGa films are microscopically inhomogeneous. Both of them contain regions with different local saturation magnetization, Curie temperatures and hence different atomic ordering.
3. High-temperature annealing of amorphous Fe_2CrGa films recovers their crystallinity with the stabilization of $A2$ type structure but does not completely recover the magnetic properties of the films to the bulk alloy level.
4. In bulk alloy, it is possible to obtain practically homogeneous structure with Hg_2CuTi type of ordering, while, in films, there is a mixture of regions with different atomic ordering including $L2_1$ and Hg_2CuTi types. For the crystalline films, the characteristic size of these regions is higher than exchange correlation length and they can be easily distinguished using FMR and VSM techniques.
5. It was shown that the Slater–Pauling rule does not work for full Heusler alloys with inverse Hg_2CuTi-type of crystalline structure.

V. Golub is thankful for support from NRFU grant 02.2020/0261.

REFERENCES

1. F. Heusler, *Verh. Dtsch. Phys. Ges.*, **12**: 219 (1903).

2. L. Krusin-Elbaum, A. P. Malozemoff, and R. C. Taylor, *Phys. Rev.*, **27**: 562 (1983).
3. K. L. Dang, P. Veillet, and I. A. Campbell, *J. Phys. F: Met. Phys.*, **7**: L237 (1977).
4. R. C. Taylor and C. C. Tsuei, *Solid State Communications*, **41**, Iss. 6: 503 (1982).
5. J. Q. Xie, J. Lu, J. W. Dong, X. Y. Dong, T. C. Shih, S. McKernan, and C. J. Palmstrøm, *J. Appl. Phys.*, **97**: 073901 (2005).
6. S. J. Lee, Y. P. Lee, Y. H. Hyun, and Y. V. Kudryavtsev, *J. Appl. Phys.*, **93**: 9675 (2003).
7. A. Vovk, S. A. Bunyaev, P. Štrichovanec, N. R. Vovk, B. Postolnyi, A. Apolinario, J. Á. Pardo, P. A. Algarabel, G. N. Kakazei, and J. P. Araujo, *Nanomaterials*, **11**: 1229 (2021).
8. M. Kogachi, T. Fujiwara, and S. Kikuchi, *J. Alloys Comp.*, **475**: 723 (2009).
9. A. W. Karbonari, R. N. Saxena, J. Mestnik-Filho, G. A. Cabrera-Pasca, M. N. Rao, J. R. B. Oliveira, and M. A. Rizzuto, *J. Appl. Phys.*, **99**: 08J104 (2006).
10. K. Seema, N. M. Umran, and Ranjan Kumar, *J. Supercond. Nov. Magn.*, **29**: 401 (2016).
11. S. Ishida, S. Mizutani, S. Fujii, and S. Asano, *Mater. Trans.*, **47**, Iss. 3: 464 (2006).
12. J. Kiss, S. Chadov, G. H. Fecher, and C. Felser, *arXiv:1302.0713v1* (2013).
13. M. G. Kostenko and A. V. Lukoyanov, *Mater. Chem. Phys.*, **239**: 122100 (2020).
14. K. Ozdogan, B. Aktas, I. Galanakis, and E. Sasioglu, *arXiv:cond-mat/0607652* (2006).
15. H. G. Zhang, C. Z. Zhang, W. Zhu, E. K. Liu, W. H. Wang, H. W. Zhang, J. L. Cheng, H. Z. Luo, and G. H. Wu, *J. Appl. Phys.*, **114**: 013903 (2013).
16. M. Farle, *Rep. Prog. Phys.*, **61**: 755 (1998).
17. K. H. J. Buschow, P. G. van Engen, and R. Jongebreur, *J. Magn. Magn. Mater.*, **38**, Iss. 1: 1 (1983).
18. R. Y. Umetsu, N. Morimoto, M. Nagasako, R. Kainuma, and T. Kanomata, *J. Alloys Comp.*, **528**: 34 (2012).
19. Y. V. Kudryavtsev, N. V. Uvarov, V. V. Klimov, and L. E. Kozlova, *J. Appl. Phys.*, **132**, Iss. 10: 105103 (2022).
20. I. Galanakis, K. Özdoğan, and E. Şaşioğlu, *AIP Advances*, **6**: 055606 (2016).
21. I. Galanakis, P. H. Dederichs, and N. Papanikolaou, *Phys. Rev. B*, **66**: 174429 (2002).
22. T. Graf, C. Felser, and S. S. P. Parkin, *Prog. Solid State Chem.*, **39**: 1 (2011).
23. G. H. Fecher, H. C. Kandpal, S. Wurmehl, and Claudia Felser, *arXiv:cond-mat/0510210v1* (2005).
24. S. Skaftouros, K. Özdoğan, E. Şaşioğlu, and I. Galanakis, *Phys. Rev. B*, **87**: 024420 (2013).